Polymer optical fiber sensors—a review

2011 Smart Mater. Struct. 20 013002

(http://iopscience.iop.org/0964-1726/20/1/013002)

Smart Mater. Struct. **20** (2011) 013002 (17pp) doi:10.1088/0964-1726/20/1/013002

TOPICAL REVIEW

Polymer optical fiber sensors—a review

Kara Peters

Department of Mechanical and Aerospace Engineering, North Carolina State University, Campus Box 7910, Raleigh, NC 27695, USA

E-mail: kjpeters@ncsu.edu

Received 2 July 2010, in final form 4 October 2010
Published 23 December 2010
Online at stacks.iop.org/SMS/20/013002

Abstract

Polymer optical fibers (POFs) have significant advantages for many sensing applications, including high elastic strain limits, high fracture toughness, high flexibility in bending, high sensitivity to strain and potential negative thermo-optic coefficients. The recent emergence of single-mode POFs has enabled high precision, large deformation optical fiber sensors. This article describes recent advances in both multi-mode and single-mode POF based strain and temperature sensors. The mechanical and optical properties of POFs relevant to strain and temperature applications are first summarized. POFs considered include multi-mode POFs, solid core single-mode POFs and microstructured single-mode POFs. Practical methods for applying POF sensors, including connecting and embedding sensors in structural materials, are also described. Recent demonstrations of multi-mode POF sensors in structural applications based on new interrogation methods, including backscattering and time-of-flight measurements, are outlined. The phase–displacement relation of a single-mode POF undergoing large deformation is presented to build a fundamental understanding of the response of single-mode POF sensors. Finally, this article highlights recent single-mode POF based sensors based on polymer fiber Bragg gratings and microstructured POFs.

(Some figures in this article are in colour only in the electronic version)

1. Introduction

Polymer optical fibers (POFs), also referred to as plastic optical fibers, have many of the same advantages as conventional silica optical fibers for sensing applications. These include low weight, immunity to electromagnetic interference and multiplexing capabilities. In general, POFs provide a much lower cost alternative to silica optical fibers, albeit with higher transmission losses. POFs have thus been applied for data transmission over short distances, e.g. local to home Internet connections and automotive applications [1]. As sensors, POFs have additional advantages, including high elastic strain limits, high fracture toughness, high flexibility in bending, high sensitivity to strain and potential negative thermo-optic coefficients. Polymers also have excellent compatibility with organic materials, giving them great potential for biomedical applications. Previously, sensors based on multi-mode POFs have been successfully applied to take advantages of these properties. Unfortunately, due to the characteristics of multi-mode fibers, these sensors are generally larger than comparable single-mode, silica fiber sensors and produce lower measurement accuracy and resolution. However, recent successes in both the fabrication of single-mode POFs and new interrogation methods for multi-mode POF sensors have enabled large deformation, high precision sensors.

The goal of this article is to highlight these recent advances and present the new sensor capabilities expected from this rapidly growing field. Additionally, the article will discuss the particular challenges and advantages to working with POF sensors as compared with silica fiber based sensors[1]. Here we will focus on strain and temperature measurements; Zubia and Arrue [3] and Bartlett *et al* [4] list many examples of chemical sensors based on multi-mode POFs. The properties of POFs are first reviewed, including multi-mode; solid core, single-mode; and microstructured, single-mode POFs. Next, practical

[1] It is assumed that the reader has previous experience with silica optical fiber sensors. If the reader is not familiar with optical fiber sensors in general, Measures [2] is a good starting reference.

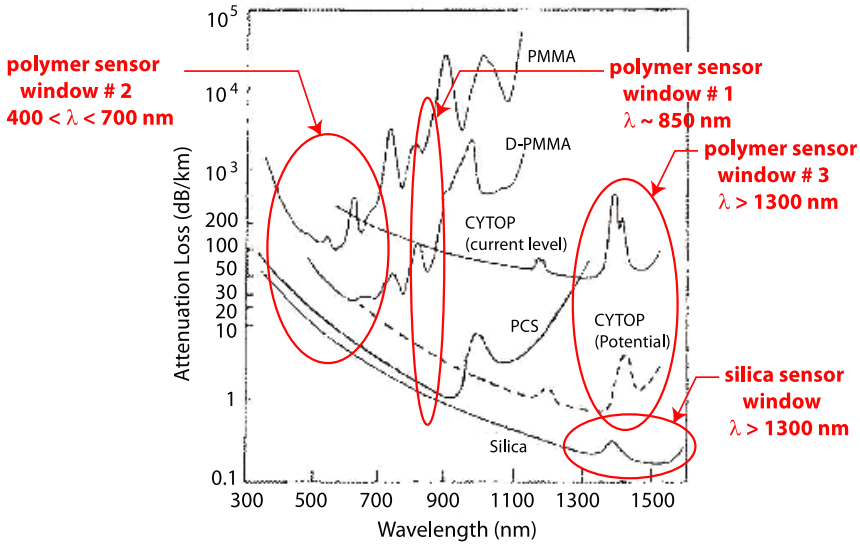

Figure 1. Attenuation loss of common optical polymers as a function of wavelength (adapted from [3], copyright (2001), with permission from Elsevier).

issues in applying POF sensors, including connectorizing and integrating them into structures, are discussed. Finally, specific sensors demonstrating the potential of each of these POF types are highlighted.

2. Properties of POFs

POFs have the same geometry as silica optical fibers, with a core, cladding and sometimes a jacket. A history of the development of POFs can be found in Zubia and Arrue [3]. A variety of optical polymers are used in the fabrication of POFs, including polymethyl-methacrylate (PMMA), amorphous fluorinated polymer (CYTOP), polystyrene (PS) and polycarbonate (PC). Ziemann *et al* [5] gives an extensive overview of common POF materials and their properties. Unlike silica optical fibers, POFs are primarily available as multi-mode fibers, which have larger diameters and propagate multiple, interacting modes. Since the larger diameter of multi-mode POFs makes them easier to handle, cleave and connect, multi-mode POF sensors are often promoted as less expensive and easier to install than their silica counterparts. While this is a true benefit for multi-mode POF sensors, care should be taken as the same does not hold for single-mode POF based sensors.

For strain measurement applications, the primary advantage to polymeric sensing materials are their ductile behavior and high elastic strain limits. For example, PMMA has an elastic limit around 10%, as compared to 1–3% for silica [6]. Lesser known advantages to POFs are their increased sensitivity to strain (strain-optic coefficient) and their potential negative thermo-optic coefficient [7]. PMMA also has a lower density (1195 kg m^{-3}) than silica (2200 kg m^{-3}), producing lower weight optical fibers [8]. The following sections review the optical and mechanical behavior of POFs necessary to understand the performance of POF based sensors.

2.1. Optical behavior

The two loss properties that define the transmission quality of an optical fiber are attenuation and dispersion. The attenuation coefficient, α, is a measure of the power loss of a lightwave propagating through the optical fiber per unit distance and is defined as

$$P(z) = P(0)10^{-\alpha z/10} \tag{1}$$

where z is the distance along the optical fiber axis, $P(0)$ is the input power of the lightwave and $P(z)$ is the output power at a distance z [9]. The sources of attenuation in optical fibers can be divided into two types: intrinsic and extrinsic [3]. Intrinsic sources are inherent to the material (e.g. material absorption, Rayleigh scattering), whereas extrinsic sources are introduced during manufacturing of the fiber (e.g. structural imperfections, microbends). The intrinsic attenuation loss of common optical polymers is plotted in figure 1 as a function of wavelength. As seen in figure 1, the primary differences in attenuation properties between POF and silica optical fibers are: (1) the inherent attenuation in optical polymers is orders of magnitude greater than those in silica and (2) at wavelengths above 700 nm, the attenuation of optical polymers increases with wavelength whereas the attenuation of silica decreases. The difference in magnitude means attenuation is often a critical factor in designing a POF sensor system, and the length of the sensor can be limited by this condition. The second difference means that POF sensors are typically designed to operate in one of three windows. The first two windows are around 850 nm, where some commercial telecoms components are available, and the visible wavelength range (400–700 nm), where the POF attenuation is minimal. In contrast, silica optical fiber based sensor systems typically operate in the near-infrared wavelength range (1300–1600 nm). As improvements are made to reduce the attenuation of POFs, a third window of operation for POF sensors is now this same near-infrared wavelength range, where existing telecoms instrumentation, originally designed for silica fibers, can be applied.

Dispersion is a measure of signal broadening due to the wavelength dependent speed of propagation through the optical fiber and it limits transmission over long distances. Several of the sensors to be discussed in this review have long gauge lengths, for which the dispersion properties of the POFs are important. As a pulsed lightwave propagates through an optical fiber it broadens mainly due to two phenomena: (1) the finite bandwidth of the laser source incorporates different wavelengths which travel at different speeds through the optical fiber (material dispersion) and (2) different modes also propagate at different speeds through the optical fiber (intermodal dispersion) [9]. The second effect is important for multi-mode optical fibers. While the material dispersion depends on the choice of polymer material and propagating wavelength, the intermodal dispersion is strongly dependent on the index of refraction profile in the optical fiber. Step index profiles have particularly high intermodal dispersion, therefore graded index profile fibers, which can lower the intermodal dispersion by a few orders of magnitude, are often used for longer distance transmission. Graded index profile POFs (GIPOFs) can therefore significantly improve the resolution of sensors based on signals transmitted over long lengths of fiber.

The most common method of increasing the core index of refraction in POFs is through doping. Doping of the core produces fibers with high numerical apertures (NA), as compared to silica fibers. The numerical aperture is defined as

$$\mathrm{NA} = \sqrt{n_0^2 - n_1^2} \tag{2}$$

where n_0 and n_1 are the index of refraction of the core and cladding respectively. This high index contrast improves the coupling efficiency of lightwaves into the POF and reduces bending losses, both advantageous for sensor applications. However this high index contrast also creates difficulties in the fabrication of single-mode fibers, which is the main reason why the development of single-mode POFs has lagged behind silica optical fibers [8]. The number of modes propagating through an optical fiber is determined by the normalized frequency,

$$V = \left(\frac{2\pi a}{\lambda}\right)\mathrm{NA} \tag{3}$$

with a the core radius and λ the wavelength of the propagating lightwave. For $V < 2.405$ only a single-mode propagates through the optical fiber, whereas for $V \geqslant 2.405$ multiple modes propagate through the optical fiber. As the NA of POFs are much higher than their silica counterparts, the core radius must be considerably smaller than for silica optical fibers in order for the fiber to be single-mode at a given wavelength. The smaller core diameter increases the scattering losses at the core–cladding interface [8]. Additionally, as the intrinsic losses of polymers are lower in the visible wavelength range, fabricating POFs to be single-mode at lower values of λ further reduces the required core diameter.

Single-mode POFs were first developed by Koike *et al* [10]. More recent advances in the fabrication of single-mode POFs with minimal attenuation levels have created the potential for single-mode POF sensors. Kuzyk *et al* [11] first fabricated optical fibers (PMMA) with a doped core that were single-mode at an operating wavelength of $\lambda = 1300$ nm. These fibers demonstrated attenuation levels of approximately 0.3 dB cm^{-1}, close to the intrinsic material attenuation for PMMA at that wavelength. Bosc and Toinen [12] later fabricated single-mode PMMA optical fibers with attenuation levels of 0.25 dB cm^{-1} at $\lambda = 1550$ nm and 0.05 dB cm^{-1} at $\lambda = 850$ nm. Finally, Garvey *et al* [13] improved the process to create single-mode POFs at $\lambda = 1060$ nm with an attenuation level of 0.18 dB cm^{-1}. Further details on advances in PMMA based single-mode POFs and active POFs can be found in Kuzyk [14]. Currently, doped, single-mode POFs are still experimental, with only one commercial manufacturer, Paradigm Optics.

An additional solution to decrease the attenuation of single-mode POFs is the fabrication of microstructured POFs (mPOFs) which have air holes in the fiber cross-section. The air fraction decreases the material in a given cross-section and therefore decreases the intrinsic losses [15]. Additionally, lightwave guidance in the mPOF can be controlled by the hole arrangement and can be considerably stronger than that in solid core, single-mode optical fibers. These two features decrease the attenuation in mPOFs significantly. Researchers at the University of Sydney have demonstrated mPOFs that are single-mode at optical wavelengths [16]. Such fibers can also function as endlessly single-mode optical fibers, meaning that they are single-mode for a wide range of wavelengths. This single-mode, low attenuation operation could enable POF sensors in the near-infrared wavelength range where many telecoms components are commercially available.

Table 1. Measured tensile properties of single-mode PMMA POFs.

Reference	Strain rate (min^{-1})	E (GPa)	ϵ_Y (%)	ϵ_U (%)
[17]	0.1–0.5	1.6–2.1	6	38
[19]	0.005	2.7	1.2	6
[18]	0.01–3.05	4.0–5.0	3.5–4.6	34
[20]	0.01	—[a]	3.3	24

[a] The POF of Law *et al* [20] is a microstructured POF with some air fraction in the core, therefore E is not comparable with the other sources.

2.2. Mechanical behavior

Tensile testing of POFs requires fixtures designed for small diameter fibers with low rigidities. Jiang *et al* [17], Kiesel *et al* [18], Yang *et al* [19] and Law *et al* [20] all report tensile testing of single-mode PMMA POFs under various strain rates and cyclic load conditions. A summary of measured properties, including Young's modulus (E), yield strain (ϵ_Y) and ultimate strain (ϵ_U), are listed in table 1. Figure 2 plots typical true stress–strain curves for a single-mode POF measured in a universal testing machine. The applied strain rate was varied from 0.01 to 3.05 min^{-1}. The failure strain for the POF was around 30% for most of the samples. The yield strain increased with the applied strain rate, as plotted in figure 3, while the initial slope of the curve also increased, although by a much lower amount.

We note that there is a large variation in material properties in table 1. Some of this variation is due to the difference in

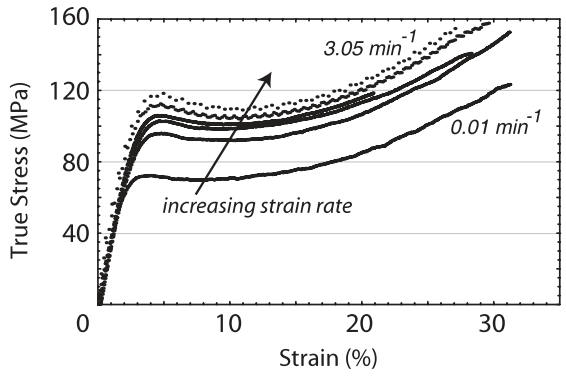

Figure 2. Measured, true stress–strain curves for single-mode PMMA doped core POF at strain rates of 0.01, 0.30, 0.60, 0.90, 1.22 and 3.05 min^{-1} [18].

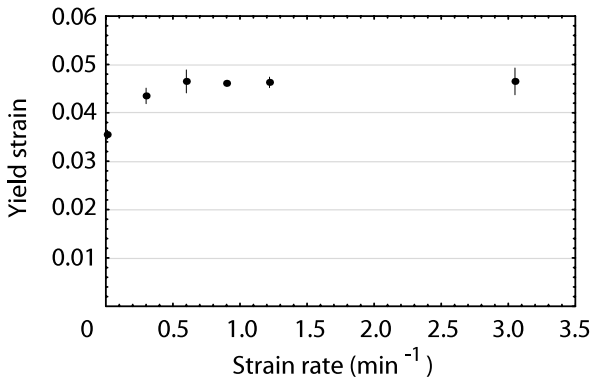

Figure 3. Yield strain versus strain rate for single-mode PMMA POF samples [18]. Error bars show standard deviation of data.

testing conditions and strain rates. However, the mechanical properties of POFs also depend strongly upon the fiber drawing process, including the drawing ratio (ratio of preform diameter to final diameter), temperature and speed [12, 17]. A detailed description of a typical drawing process for single-mode, doped PMMA POFs can be found in Jiang *et al* [17]. An important factor in the fiber mechanical behavior is the annealing process to remove internal stresses. During the drawing process, the polymer molecules align in the axial direction, creating anisotropic material properties. In addition to changing the mechanical properties, anisotropy in the optical fiber creates birefringence in the fiber cross-section which reduces the lightwave transmission quality through the optical fiber. This stress relaxation also causes small cracks to appear in the radial direction [21]. This effect is enhanced at elevated draw temperatures. Jiang *et al* [17] annealed polymer bulk materials above the glass transition temperature for one week before drawing to ensure they were isotropic. After drawing, the POFs were annealed at 95 °C, just below the glass transition temperature to release the residual stresses. Observation of the failure modes of unannealed POFs demonstrated a higher strength than the annealed fibers and a brittle failure. The POFs fractured in the form of multiple cracks and splitting along the axis of the POF, typical of anisotropic materials. In contrast, the annealed fiber failed in a ductile manner, typical of an isotropic material. Finally, the dopant concentration used to increase the index of refraction of the POF core can also change the ductility of the POF slightly [17]. In summary, it is important to calibrate the specific POF to be used for a sensing application, as the properties between POFs are not as consistent as between silica fibers for telecom applications.

Large *et al* [6] studied the stress relaxation and creep behavior of PMMA single-mode (microstructured) POFs. While the stress relaxation effect was not significant (measured through the change in resonant wavelength of a long period grating due to the stress-optic effect)[2], the strain under constant stress (creep) was significant and a function of the applied strain. These results emphasize the viscoelastic behavior of polymer fibers. Depending upon the sensor mounting conditions, such effects could play a significant role in the response of a POF sensor.

Aging due to high temperature or humidity environments is an important challenge for some POF sensor applications [22]. The maximum operating temperatures for POFs are typically in the range of 80–100 °C [3]. However, elevated temperatures below the maximum operating temperature can cause the POF to become brittle and disintegrate over time. In addition to weakening the POF, these changes increase the attenuation in the POF and can affect the dopant properties, changing the refractive index profile in the cross-section [22]. Amongst the optical polymers, CYTOP is the most thermally stable [22]. Humidity is another important concern affecting the long term stability of POFs, and is further emphasized at elevated temperatures. Ziemann [23] provides detailed results of extended temperature and humidity testing of POFs. In general, the optical transmission fell rapidly over a period of a few days, followed by stable transmission over several weeks. After this stable period, the optical transmission decreased rapidly to zero due to the rapid absorption of moisture by the polymer. During testing in which the humidity was removed during this period, the transmission returned almost to that of the stable period. Temperature also plays a strong role on the fatigue life of POFs. Ziemann *et al* [22] demonstrated that low or elevated temperature environments accelerate power transmission losses due to fatigue cycling in bending of a multi-mode POF.

2.3. Strain and temperature sensitivity

To measure the strain sensitivity of an optical fiber for sensing devices, we typically subject the fiber to a pure axial strain. We define the strain sensitivity as the phase change in a lightwave propagating through the optical fiber per unit length of elongation. Based on the Pockel's constants for bulk PMMA, the strain sensitivity of a PMMA POF is theoretically predicted to be 132.6×10^5 rads m^{-1} [7]. This is about 15% larger than the strain sensitivity of bulk silica, which is 115×10^5 rads m^{-1}. Likewise, we define the thermal sensitivity to be the phase shift in a lightwave propagating through the optical fiber per unit change in temperature per unit length of the fiber. For bulk PMMA, the thermal sensitivity is calculated

[2] The stress relaxation in microstructured POFs may be less pronounced than that of solid POFs due to the large air fraction in the fiber cross-section.

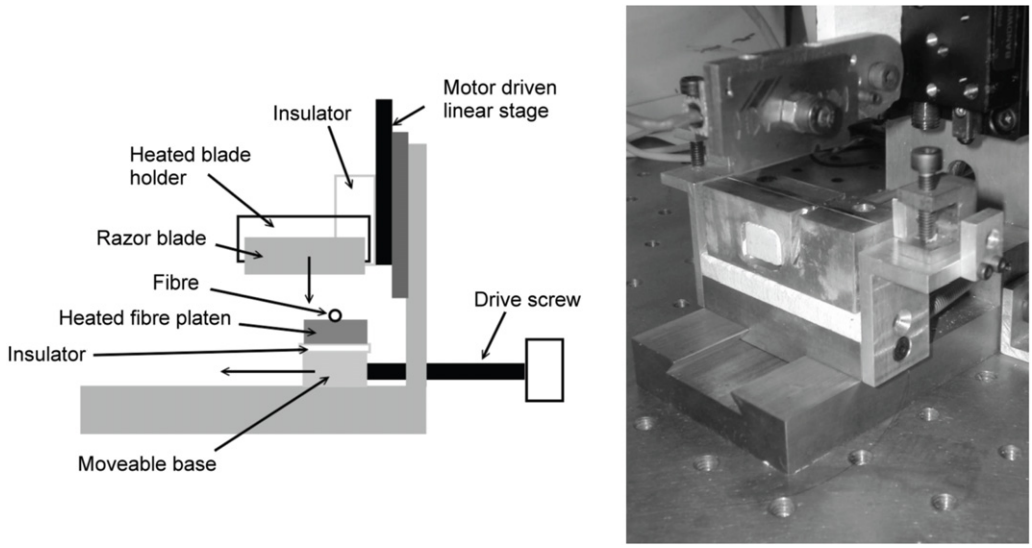

Figure 4. Hot-knife cutter at the University of Sydney (reprinted from [26], copyright (2006), with permission from Elsevier).

to be -154.3 rads m^{-1} K^{-1}. This is not only larger in magnitude that of silica (98.8 rads m^{-1} K^{-1}), but is also of the opposite sign. This negative thermo-optic coefficient, which is the case for some polymers, will present new possibilities for temperature compensation in strain sensors, as will be discussed later. On a final note, these sensitivities are based on the linear response of the optical fiber and therefore apply to small strain and temperature conditions. Due to the high yield strain and strong nonlinear mechanical properties of the POFs, the nonlinear phase response with strain should be considered as early as 1% axial strain [18]. Analytical predictions and experimental measurements of the nonlinear strain response on PMMA POFs are presented in section 5.1.

3. Practical application of POF sensors

3.1. Connectorizing POF sensors

One of the most significant, practical challenges in applying some POFs as sensors is in preparing the POF endfaces for connection to other optical fibers or instrumentation. On the one hand, a wide range of connectors are commercially available for multi-mode POFs [24]. Due to their large diameter, these POFs are relatively easy to cut and handle during preparation. Furthermore, the large core size reduces the core alignment requirements. On the other hand, the extremely small core size and flexibility of polymer materials makes connecting single-mode POFs difficult. The high attenuation properties of single-mode POFs often requires that the POF sensor be connected to silica optical fibers as leads to and from the instrumentation. Microstructured, single-mode POFs have larger core diameters, however the presence of small holes in the cross-section requires better control to prevent debris from clogging the holes or thermally induced collapse of the holes [25]. In this section we discuss some of the successful and unsuccessful methods applied to connectorizing single-mode POFs. The examples presented have all considered PMMA, single-mode POFs.

For any optical fiber, the endfaces must first be cleaved to produce a surface that is smooth and perpendicular to the axis of the optical fiber. For silica optical fibers, cleaving is performed by first notching the outer surface to produce a micro-crack in the fiber cross-section and then bending the optical fiber to propagate the crack across the cross-section. This well established procedure produces a smooth fracture surface perpendicular to the fiber axis. Due to the viscoelastic nature of polymers and their low stiffness, applying this cleaving method to POFs produces a combination of cutting and tearing which reduces the quality of the cleaved surface [20]. The ductile behavior of the polymer produces plastic deformation at the fracture surface which warps the cross-section. When the PMMA is in a brittle state, the material anisotropy creates turning of the crack front and chipping, creating debris that is dragged over the fracture surface. Alternative methods must therefore be applied for preparing the POF endfaces and connecting them to optical fibers.

The most successful method for practical field cleaving of single-mode, PMMA POFs has been through hot-knife cleaving, first applied to single-mode microstructured POFs by Law *et al* [20, 26]. Figure 4 shows a schematic and photograph of the cutter used by the authors in which the blade and platen are heated separately. The POF is mounted on the platen and allowed to reach an equilibrium temperature before cutting. The cutting speed is controlled with a stepper motor and the blade cutting surface rotated so that each POF is cut with a pristine blade surface. Law *et al* [20, 26] performed a careful analysis of the cleaved POF endface for multiple fiber temperatures, blade temperatures and cutting speeds. The PMMA was ductile in the range 25–100 °C, with a transition in material structure around 60 °C (the glass transition temperature was around 115 °C). The authors found that the best results were obtained when the blade temperature was slightly lower than the fiber temperature and both were around this structural transition temperature. Furthermore,

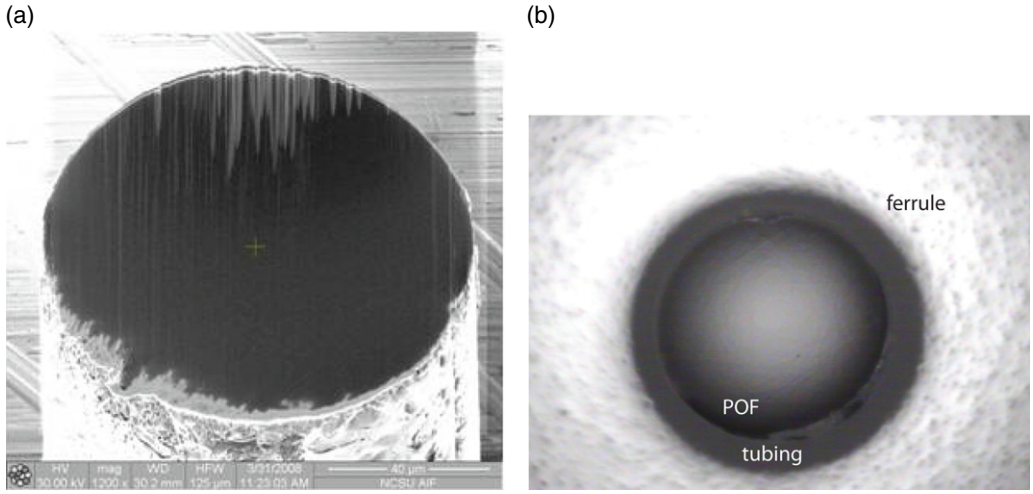

Figure 5. Optical microscopy images of (a) focused ion-beam cleaved cross-section after final polish (image taken at 52° tilt angle) and (b) FC connector cross-section region near ferrule (reprinted from [27], copyright (2009), with permission from Elsevier).

lower blade cutting speeds produced better endface surfaces. The optimal results were obtained for the following ranges: fiber temperature 70–80 °C, blade temperature 60–70 °C, blade speed 0.07–0.5 m s^{-1}. The POF also required about 90 s to equilibrate to the platen temperature before cutting.

Abdi *et al* [27] performed hot-knife cleaving of solid core, single-mode PMMA POFs and found two optimal ranges for cutting: (1) fiber temperature 30–40 °C, blade temperature 80 °C and (2) fiber temperature approximately 80 °C, blade temperature 80 °C. A negative side effect to heating the optical fiber above 80 °C for more than 6 min was embrittlement of the POF, demonstrated by tensile testing of POFs with and without heat exposure. Therefore the 30–40 °C fiber temperature range was recommended for practice. The difference in temperature ranges between this and the work of Law *et al* [20, 26] highlights the role of different fabrication processes on the optimal temperature range for individual single-mode POF configurations. Finally, chilling of the POF to low temperatures causes chipping of the optical fiber and produces poor quality surfaces [20, 27].

Two other successful methods of cleaving single-mode POFs are UV laser cleaving and focused ion-beam machining [25, 27]. Both of these methods produce the highest quality endfaces of the POFs for laboratory environments, however neither is practical for rapid connecting of sensors in field applications. Figure 5(a) presents an optical microscopy image of a focused ion-beam cleaved cross-section.

Once the POF has been cleaved, the second step in preparing the sensor is to connect the POF to either another single-mode POF or to a silica, single-mode optical fiber. The success of this coupling depends on the core alignment of the fibers, the gap distance between the two fibers, the degree to which the endfaces are parallel and the difference in core sizes between the two fibers. For laboratory experiments, free-space coupling of lightwaves into the POF clearly produces the lowest coupling losses [6, 7, 28]. However, in most field applications a more ruggedized connector is required that does not require precise alignment of the fibers and prevents the fibers from moving relative to one another. The high attenuation of single-mode POFs also means that the sensor gauge length is often short and these connectors need to be mounted on the structure itself.

The most successful approach to achieve a field suitable connector with relatively low loss has been to first cleave the POF as discussed above and then to glue it into a ferrule for coupling. Abdi *et al* [29] coupled pre-cleaved, single-mode POFs to single-mode silica optical fibers using ferrules from standard single-mode FC connectors. The single-mode POF diameter was 125 μm, which was ideal for alignment of the fibers in the ferrule. This connector was then glued to the surface of tensile specimens and survived beyond the application of 10% axial strain to the POF. A second approach, based on inserting the POF into a complete FC connector and polishing the endface, was unsuccessful [27]. The PMMA material was more flexible than the surrounding ferrule, resulting in movement of the POF within the connector during polishing. An optical microscopy image of a representative connector endface is shown in figure 5(b). Typically, the POF fractured during the polishing process, resulting in a POF cross-section which was not coplanar with the ferrule surface. Additionally, the submersion of the POF surface prevented the FC connector from transmitting lightwaves effectively.

The larger core size of single-mode microstructured POFs means that they are often better suited for connection to multi-mode rather than single-mode silica fibers. Lwin and Argyros [30] measured coupling losses between single-mode microstructured POFs of various core diameters and multi-mode, silica optical fibers (100 μm core diameter) using commercial SMA connectors. The input losses from the silica fiber to the microstructured POF were primarily due to overfilled launch conditions since the silica fiber core diameter was considerably larger than the POF core diameters. In the output coupling from the POF to the silica fiber, overfill did not occur and the loss was negligible. In total, coupling losses up to 1.5 dB were measured at a wavelength of 650 nm for the 24 μm core POF; this is below the POF data communication standards of 2 dB.

Table 2. Potential issues for the embedding of POFs in common structural materials.

Issue	Description	Silica optical fiber	Polymer optical fiber
Elevated processing temperatures	Elevated temperatures and humidity applied during curing of polymer matrix composites and developed internally during curing of concrete could damage optical fiber material	Coatings such as polyimide successfully protect the silica fiber from processing temperatures and moisture ingress	Elevated temperatures and humidity can artificially age polymers. The lack of protective coating could be an issue
Bond strength	For an accurate strain measurement the optical fiber must be well bonded to host material	The bond strength varies as a function of optical fiber coating and host material	The bond strength varies as a function of optical fiber coating and host material (see section 3.2)
Disturbance to host material geometry	Optical fibers embedded between laminae in a composite laminate bend the laminae and can create resin rich zones or air pockets, reducing the integrity of the laminate	The relatively small diameter of silica fiber lessens this effect (but coating diameter must also be considered)	The larger diameter of multi-mode POFs increases this effect. Small diameters single-mode POFs would be comparable to (or less than) silica optical fibers
Microbending	Excessive microbending of the optical fiber creates optical transmission losses	Bare silica fiber is highly sensitive to microbend losses, however stiff coatings such as polyimide prevent excessive microbending	The high NA of the POF makes it less sensitive than silica optical fibers to microbending losses
Residual stresses	Residual stress in the host material developed during processing compresses the optical fiber and can reduce the optical power transmission	Coatings such as polyimide protect the silica fiber from significant residual stresses	The flexibility of the polymer and lack of coating makes the POF more susceptible to crushing. The coefficient of thermal expansion of optical polymers are close to that of epoxy resins, reducing residual thermal stresses when embedded in composite laminates

3.2. POF integration into material systems

Similar to silica optical fiber sensors, POFs can be integrated into structural materials for *in situ* strain and temperature monitoring. While many of the integration issues are similar between silica fiber and POF based sensors, some differences are important, as highlighted in table 2. In this section, we summarize the knowledge gained from three recent studies on POF sensors embedded in material systems; one in a concrete infrastructure system, one in a geotextile and the other in a glass fiber–epoxy laminate.

Kiesel *et al* [31] investigated the suitability of single-mode POF sensors for *in situ* monitoring of civil infrastructure systems. Single-mode, PMMA POFs (diameter 115 μm) were partially embedded during casting of three typical civil structural materials: mortar, hydrostone, and cement paste. The POFs were then pulled from the cast specimens at a rate of 2.5 mm min^{-1} in a tensile testing machine to evaluate the bonding strength. Typical measured force versus displacement curves for each of the three material types are plotted in figure 6. The POF fiber embedded in mortar broke at the exit point of the fiber at approximately 1.4 N. The total slippage of the POF from the mortar was relatively low. The total slippage of the POF embedded in hydrostone was significantly higher that of the mortar specimen. At the same time, the POF did fail at a higher load of 2.5 N. In the cement paste specimen, the POF yielded and then broke at the maximum load of 2.7 N before any significant slippage had occurred. From these results we can infer that the relatively large particle size of the mortar caused premature failure of the POF, while the POF did not sufficiently bond to the hydrostone. The cement paste was therefore the optimal material system in which to embed the POF due to the strong bond between the cement and the POF. Presumably, this is due to the small particle size of the cement paste.

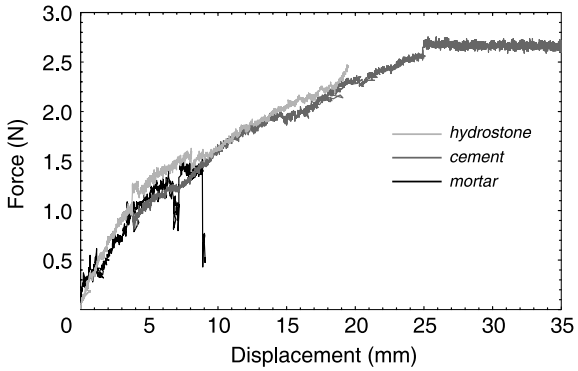

Figure 6. Force versus displacement curve for pullout tests of single-mode POF embedded in several structural materials [31].

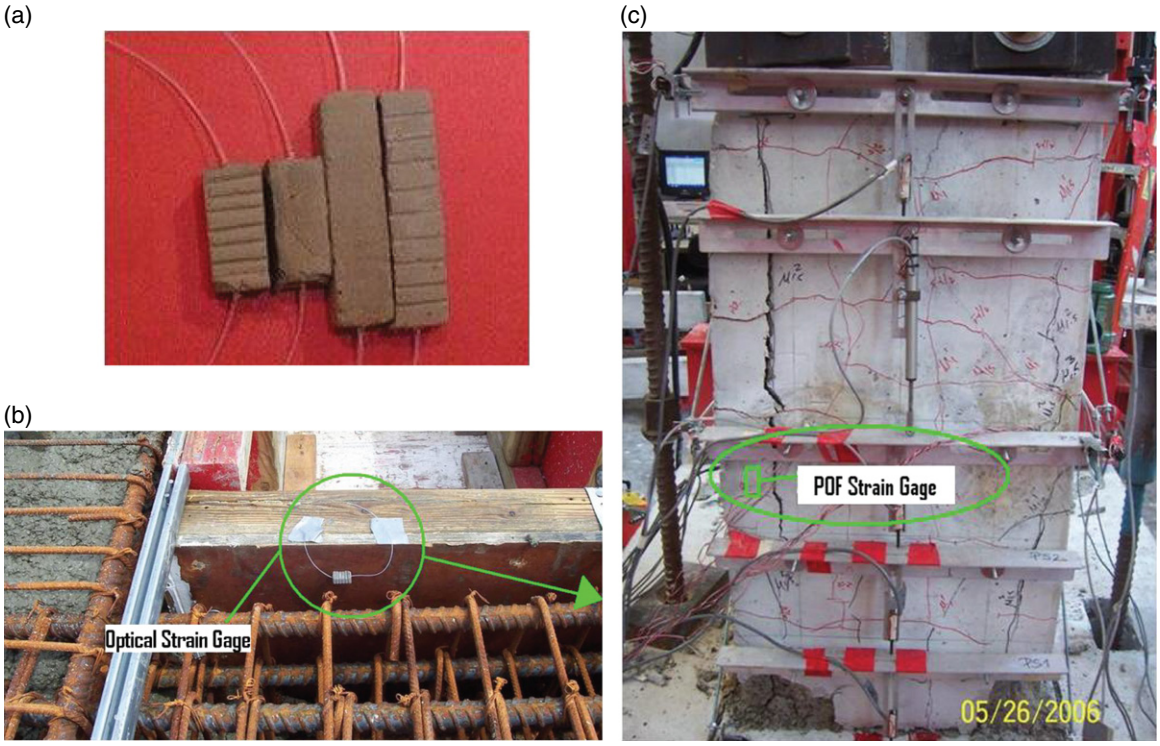

Figure 7. Embedding of single-mode PMMA POF in concrete structural component. (a) POFs embedded in pre-cast concrete blocks; (b) fixture of pre-cast block to frame for casting of the concrete structure; (c) concrete structure after failure. (Photographs courtesy of Omid Abdi.)

The second concern when embedding POF strain gauges in concrete structures is the large shrinkage of the concrete during cure and potential optical power transmission losses in the POF as a result. To mitigate the effects of the residual stresses, the POF was first embedded in a small pre-cast concrete block, as shown in figure 7(a). The block was then fixed to the frame before casting of the reinforced concrete structural component, as shown in figure 7(b). The ribbed edges of the small blocks permit better bonding of the pre-cast block to the surrounding concrete. No significant loss in optical transmission was measured after embedding and curing of the concrete. The pre-cast block was then embedded in the reinforced concrete structure, which was then loaded until failure (see figure 7(c)). The POF showed no visible damage after the final stages of the test.

Liehr *et al* [32] embedded a PMMA multi-mode POF directly into a geotextile. In this application, the POF was free to slide within the woven textile material. The sensors survived the installation process of embedding the geotextile into a railway embankment and were still functioning properly after nine months of operation.

Schukar *et al* [33] recently embedded multi-mode POFs in glass fiber–epoxy laminates to evaluate the influence of the POF on the laminate microstructure and potential changes to the POF material at elevated temperatures. The laminates were cured at a constant temperature of 60 °C. Three different diameter multi-mode POFs were embedded: 1 mm, 500 and 250 μm. Throughout the curing process, the POF backscatter was measured using an optical time domain reflectometry (OTDR) system and revealed no changes to the fundamental properties of the POF (PMMA) at this curing temperature and residual stress level. The 1 mm diameter POF created too much of a disturbance to the laminate geometry and resulted in large air pockets surrounding the POF, therefore it was deemed not suitable for integration. The amount of air and epoxy resin surrounding the 500 and 250 μm diameter POFs was significantly less. As expected, the least disturbance was created by the 250 μm POF. However, this fiber was not of a standard size and therefore had a much larger attenuation than the more standard 500 μm POF. Therefore, the 500 μm POF was selected as the optimal diameter for embedding. In comparing the POFs diameters to standard silica optical fibers, it should be noted that the POFs did not require an additional coating. Whereas standard silica optical fibers are 125 μm in diameter, with added coatings (e.g. polyimide) the actual embedded fiber diameter is often in the range 200–250 μm.

Finally, Schukar *et al* [33] also tested a laminate to failure in tension with an embedded 500 μm POF to evaluate the bonding between the POF and host material [33]. The POF survived beyond the failure strain of the glass fiber–epoxy composite (1.6%) and continued to provide good transmission even after failure of the laminate. The measured increase in backscattering loss of the POF before and after the laminate failure was only 0.6 dB. Figure 8 shows an example specimen after testing with an embedded POF bridging the failure surface of the laminate. These results indicate that the POF retains its ductility even after the elevated temperature cure of the laminate.

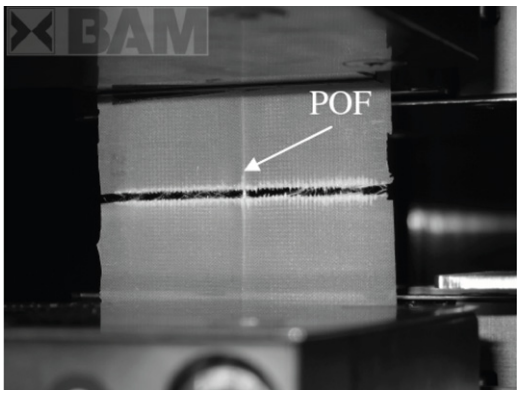

Figure 8. Photograph of laminate after tensile failure, with visible embedded POF [33].

4. POF sensor examples—multi-mode

As mentioned previously, multi-mode POFs are commercially available, relatively inexpensive and easy to handle and connect. In this section we review sensors based on multi-mode POFs ranging from simple, inexpensive sensors based on optical power loss to more sophisticated distributed sensing methods based on the measurement of POF backscattering properties. A third alternative, based on time-of-flight measurements through the multi-mode POF is also introduced. Each of these sensors has the same benefits over comparable silica optical fiber based sensors, in that they can be applied in high strain environments where silica optical fibers would fail.

4.1. Optical loss based POF sensors

The earliest studies using POFs for strain sensing were based on measuring optical transmission losses in the POF due to strain concentrations near the sensor. For example, Takeda [34] embedded multi-mode, PMMA POFs in carbon fiber–epoxy laminates for the detection of cracking. Light from a light emitting diode (LED) was coupled into the POF and the output power measured with a photodetector. This is a very inexpensive sensor and was shown to be highly sensitive to the local crack density in the laminate as the laminate was loaded in tension. Due to its high strain limit, the POF survived beyond the failure of the laminate. Although the sensor was able to detect the presence of cracks, spatial information was not obtained and its sensitivity to other parameters was not evaluated.

To increase the sensitivity of the optical transmission loss to applied strain, Kuang *et al* [35] removed a portion of the cross-section of a 980 μm diameter, multi-mode, PMMA POF. The optical transmission was measured in the same manner as in Takeda [34]. The POF was adhered to a metallic specimen and acted as a strain gauge through bending of the POF. Two configurations were applied: (1) a test in which the POF was along the axis of a beam during bending and (2) the POF was mounted on a beam in a curved path such that tensile and compressive loading of the beam caused a change in curvature of the POF. The resulting POF cross-section was not symmetric, therefore the bending direction could also be identified. The POF was not very sensitive to tension along the POF axis. The sensor demonstrated a linear decrease in transmitted power with increase in bending curvature and a linear increase in transmitted power with decrease in bending curvature. No hysteresis was observed in the strain range measured (up to 12 millistrain). Kuang *et al* [36] later applied this sensor to measure the free vibration response of a carbon fiber–epoxy laminated beam to detect changes in the damping behavior due to damage. A second application was the detection of cracks in concrete beams loaded in bending [37]. In this application, the presence of cracks produced localized necking of the POF and therefore large decreases in optical transmission. For the POF surface mounted along the beam, the total optical transmission loss was approximately linearly related to the number of cracks along the beam. Some deviation in this relation was obtained towards the end of the test, presumably due to crack widening at some crack locations. Discrimination of these two effects could not be obtained with an integrated measurement.

Other researchers have increased the sensitivity of the transmission power loss to axial strain by chemical tapering of the POF [38], removing a curved section (groove) of the cross-section [39] and combining multiple grooves in the cross-section with bending of the cross-section [40]. Remouche *et al* [41] took advantage of the large thermo-optic coefficient of polymers to design a temperature sensor based on a bent length of POF. The optical loss through the bend changed as a function of index of refraction of the polymer and therefore the applied temperature. The thermal sensitivity of this sensor is theoretically one order of magnitude greater than an equivalent silica optical fiber based sensor.

4.2. Backscattering based POF sensors

To perform a more detailed analysis of the optical losses, Husdi *et al* [42] calibrated the optical time domain reflectometry (OTDR) response of several standard multi-mode, large diameter (1 mm), step index PMMA POFs. In order to capture the weak backscattering levels, the authors applied a specially designed photon-counting detector, operating at a wavelength of 650 nm. The POFs were subjected to bending, clamping, twisting, axial strain and temperature loadings. As expected, the spatial resolution depended on the launch NA and the modal dispersion in the POF. One interesting observation was that a permanent 'memory effect' appeared in the OTDR response in which the measured losses remained after the load was removed [43]. This memory effect could be used to measure the maximum strain achieved during a loading–unloading cycle. It was presumed that this memory effect is due to plastic deformation occurring in the POF after approximately 5% axial strain.

Extending the OTDR measurement of POF backscatter to field applications, Liehr *et al* [32] embedded large diameter, multi-mode PMMA POFs in textiles for the monitoring of geotechnical and masonry structures. The geotextiles, examples of which are shown in figure 9(a), were embedded in a railway embankment for the monitoring of soil displacements. The large core diameter and NA multi-mode POFs applied allowed easy connection to and handling

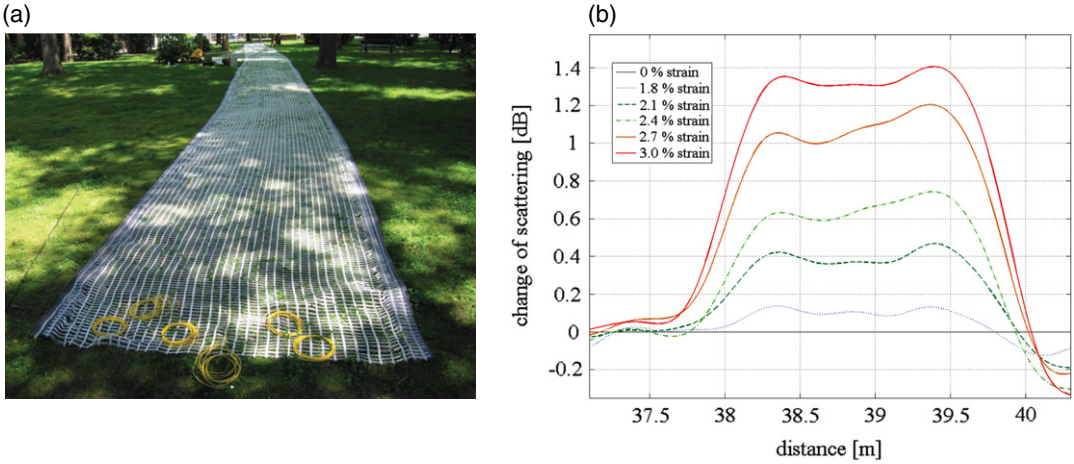

Figure 9. (a) Sensor integrated geotextiles; (b) change of backscattered signal relative to a reference measurement along a 1.8 m section of a tensile loaded, perfluorinated GIPOF [44].

of the sensors at the construction site, while the use of the standard POF itself as the sensor permitted monitoring of a large area at low cost. Additionally, the high ultimate strain of the PMMA allowed the POF to elongate with the large soil deformations. In a second application, the POF was embedded into a wearable belt for monitoring the respiratory movements of a patient in environments where electrical signals cannot be used by the sensors, for example in magnetic resonance imaging facilities [45]. The performance of the POF sensor was comparable to silica optical fiber based macrobending and Bragg grating sensors, which were also tested. One major advantage of the POF in this configuration was its compatibility with the more than 50% elongation requirement for the textile.

The use of PMMA POFs for OTDR measurements was limited by the attenuation and dispersion characteristics of the fiber. While strain measurements were obtained up to 40% axial elongation of the fiber, the attenuation reduced the length of fiber that could be interrogated to 100 m [32]. Replacing the POF with a low loss, graded index, perfluorinated POF (PF-GIPOF) significantly improved both the measurement resolution and maximum fiber length as a result of the reduced dispersion and attenuation in the fiber (see section 2.1). This fiber permitted sensor lengths up to 500 m and could be interrogated with standard, telecom components (at 1072 and 1311 nm). A sample backscattered signal for this fiber is plotted in figure 9(b). Furthermore, the authors improved the measurement resolution to 10 cm and calculated the cross-correlation of the characteristic backscatter profile of the fiber for distributed length change measurements. The PF-GIPOF fiber was also less sensitive to bending of the fiber and did not demonstrate a reduction in signal for bend radii greater than 15 mm.

Liehr *et al* [46] later measured the backscatter of the PF-GIPOF using incoherent optical frequency domain reflectometry; this increased the measurement resolution of the strain measurements. The OFDR technique was also extended to dynamic measurements up to 2 kHz [47]. While the presented data achieved a length change resolution of 1 μm and large dynamic range, the experiments were performed with single-mode silica optical fibers and the results for POFs have yet to be reported at the time of this article.

Kreger *et al* [48] applied swept-wavelength interferometry (SWI) to measure the backscattered signal in a multi-mode POF. This interrogation method is fundamentally different from OTDR techniques, since SWI measures phase shifts rather than amplitudes in the backscattered signal. SWI provides a much higher spatial resolution (20 mm in the case of [48]) along the optical fiber, as compared to OTDR measurements. While the spectrum of the backscattered signal is random, it is deterministic, and local changes in temperature or strain create a wavelength shift in the response, similar to the effect measured by fiber Bragg grating sensors. Kreger *et al* [48] achieved a 3.4 $\mu\epsilon$ strain resolution and a 0.6 °C temperature resolution applying the technique to a 50 μm core diameter graded index, multi-mode POF. The cost of this increased strain and temperature resolution is that changes in modal distributions within the multi-mode optical fiber create noise in the signal. This modal dispersion limits the length of POF that can be interrogated. Kreger *et al* [48] launched lightwaves into the POF using a low NA single-mode connector, thus only the low order core modes of the POF were populated over a few meters of the optical fiber. Kreger *et al* [48] propose to apply the measurement to a single-mode POF, however, as attenuation levels are currently much higher in single-mode POFs, the maximum sensor length may be further limited. Swept-wavelength interferometry would therefore be appropriate for high accuracy, high spatial resolution applications with shorter sensor lengths than those of OTDR applications.

4.3. Time-of-flight POF sensors

For some structural applications, it is sufficient to measure the integrated strain along the POF. The time-of-flight measurement provides sufficient displacement resolution for a full-scale structure, yet at orders of magnitude lower cost than the OTDR and similar systems described above. Gomez *et al*

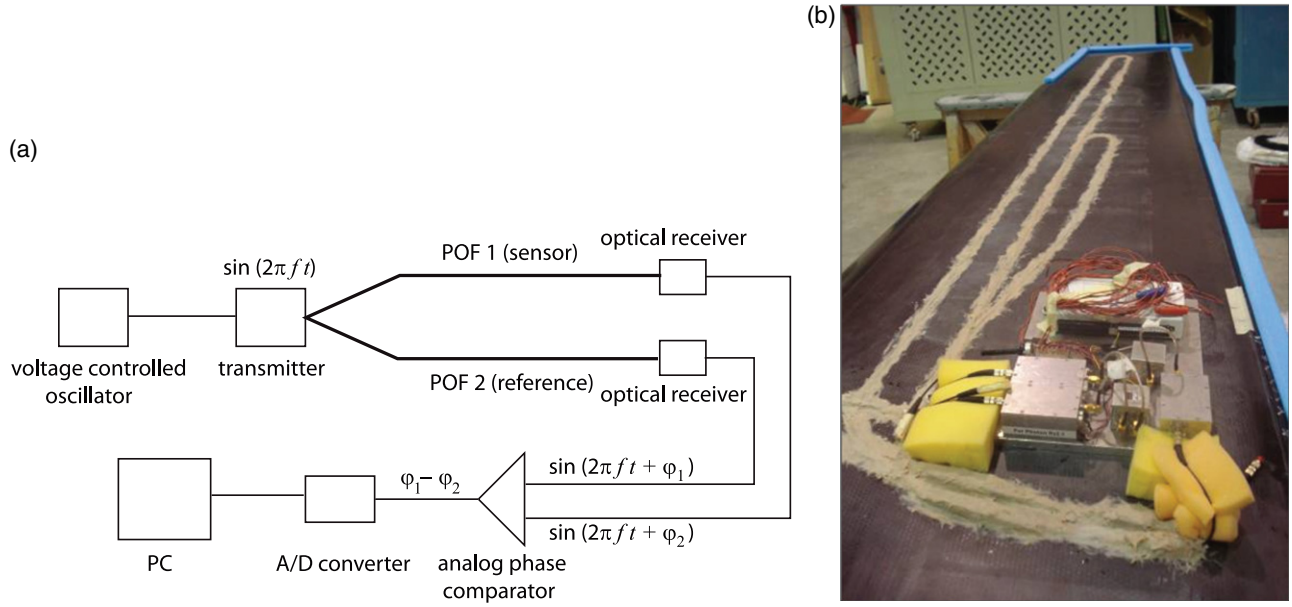

Figure 10. (a) Schematic of voltage-controlled oscillator interrogator used for time-of-flight measurements. (b) Photograph of upper side of aircraft flap showing POF adhered to surface and prototype instrumentation [49].

[49] and Durana *et al* [50] applied time-of-flight measurements to monitor the global displacement of a vibrating aircraft wing flap. A diagram of the voltage-controlled oscillator (VCO) driven interrogator is shown in figure 10, along with a photograph of the aircraft flap with the surface mounted sensor POF. In this configuration, the phase of a sinusoidally intensity modulated optical sensor signal is compared to that of a similarly modulated reference fiber signal. The relative phase shift between the signals is linearly dependent upon the strain and temperature difference between the fibers, integrated along the length of the fibers. The reference fiber (also POF) can be used for temperature or other signal compensation. The phase of the optical sensor signal could also be compared to the original electrical signal used to modulate the laser source if a reference fiber is not required [51]. The key difference between this and classical, phase based, interferometric optical fiber sensors is that the phase shift measurement is of the intensity modulation from the VCO and not phase shifts of the propagating lightwave.

The constant frequency modulation, combined with digital filtering of the signal, provides a high-resolution time-of-flight measurement, all based on low cost, commercially available telecom components and multi-mode POF. The system is also portable, durable (since no moving parts are required) and has relatively low power requirements. The resolution of the elongation measurement is determined by the resolution of the oscilloscope, the filter and noise level. The measurement displacement range, on the other hand, is determined by the oscillator modulation frequency, and can be quite large compared to other interrogation methods.

5. POF sensor examples—single-mode

As described in section 2, single-mode POFs have recently been fabricated, both in solid core and microstructured designs. The emergence of these optical fibers has created the potential for polymer based, high precision, large deformation optical fiber sensors for a variety of applications. In this section we review recent examples of single-mode POF strain and temperature sensors. To begin, we present the simplest sensor design, that of using the single-mode POF itself as an arm in a phase based interferometer. Calibration of the response of this sensor configuration can be used not only to measure strain or temperature, but also to reveal a fundamental understanding of the opto-mechanical response of the POF under large deformations. This response model could be applied to predict the response of any intrinsic, single-mode POF sensor design. Therefore the response of this sensor configuration will be discussed in detail. Afterward, we present recent successes in the fabrication of fiber grating based sensors written into single-mode POFs to provide localized, multiplexed sensing capabilities. Finally, we present new directions in the fabrication of mPOF based sensors which are expected to extend POF sensing into new domains.

5.1. In-fiber POF Mach–Zehnder interferometer

Kiesel *et al* [28] recently demonstrated coherent interferometry in a single-mode POF in-fiber Mach–Zehnder interferometer up to 15.8% elongation of the POF. This strain range is well beyond that previously measured with silica optical fiber sensors. As expected, the measured phase–displacement sensitivity was not constant over the usable strain range. It is important to both calibrate and understand the source of nonlinearities in the phase response of the POF.

Silva-Lopez *et al* [7] first measured the sensitivity of doped single-mode POFs to strain and temperature. The POFs were designed to be single-mode at 850 nm, with an acrylic cladding ($n = 1.4905$) and doped PMMA core ($n = 1.4923$). The authors operated the fibers with a visible light source at

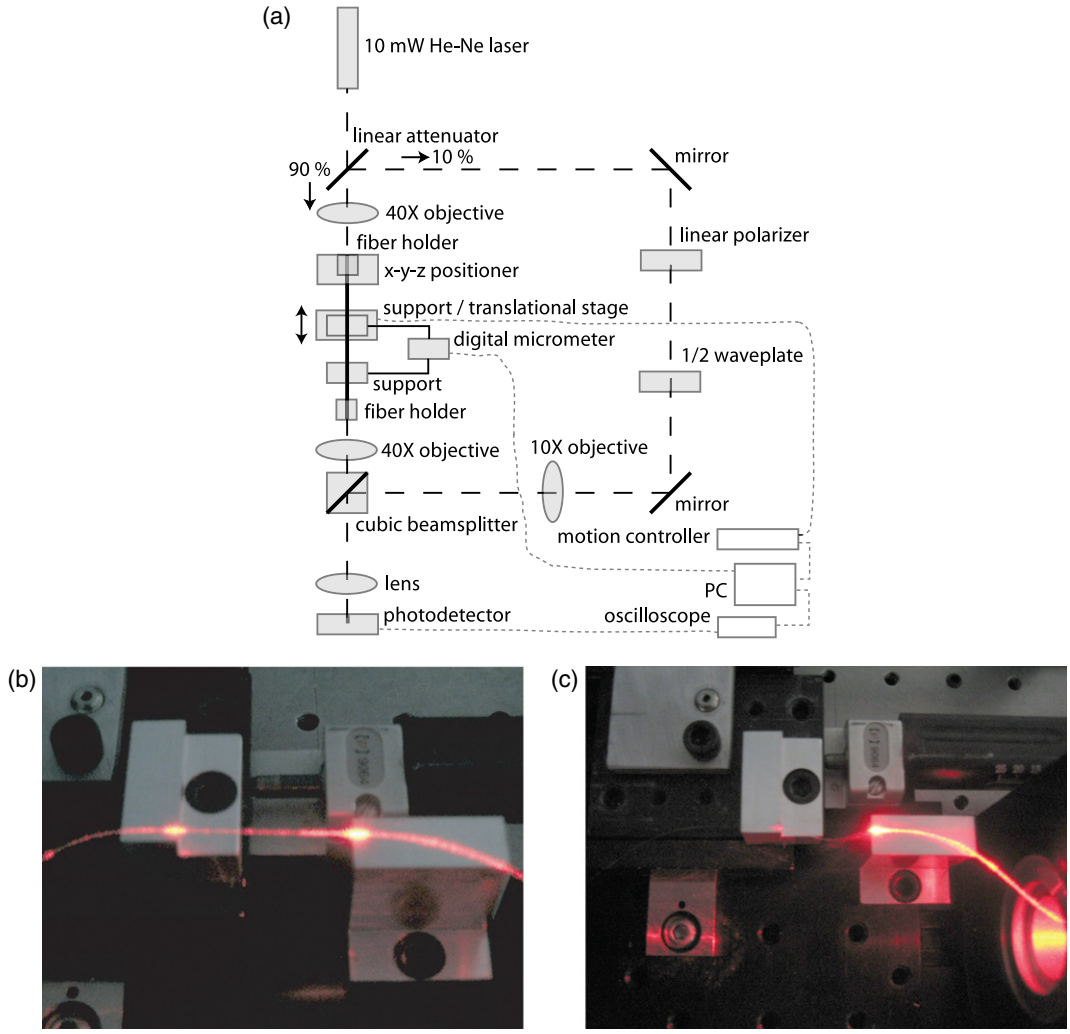

Figure 11. (a) Mach–Zehnder interferometer for the measurement of POF phase–displacement sensitivity. (b) POF during loading with uniform visible light attenuation. Bright spots are locations where POF is glued to supports. (c) POF during loading localized visible light attenuation.

$\lambda = 632$ nm, outside of the single-mode region, however they only observed the fundamental mode propagating through the fiber. Using a Mach–Zehnder interferometer arrangement and loading the optical fiber on a translation stage, they measured a phase sensitivity to displacement of 1.31×10^7 rad m^{-1}. This phase sensitivity is in good agreement with the properties of bulk PMMA discussed earlier. The measurements of Silva-Lopez *et al* [7] were made in the strain range of 0–0.04%, which is a limited portion of the strain range over which single-mode POF sensors have the potential to be applied.

To extend this strain range, Kiesel *et al* [18] derived a formulation for the phase–displacement response of an optical fiber in uniaxial tension considering large strain magnitudes. When including nonlinear behavior in the phase–displacement relation, the authors included the finite deformation of the optical fiber and potential nonlinear photoelastic effects, both up to second order in strain. Kiesel *et al* [18] then performed a series of tests on single-mode POFs to calibrate the mechanical nonlinearities and demonstrated their importance at as little as 1% axial strain in the POF. Finally, Kiesel *et al* [52] measured the phase–displacement response of the POF specimens over the maximum strain range. Figure 11 shows the Mach–Zehnder interferometer arrangement applied to measure the POF phase–displacement sensitivity. The sensor arm was a length of the single-mode POF, with the gauge length to be loaded glued between two supports. The reference arm was through air and had an adjustable length, to compensate for the index of refraction difference, and an adjustable attenuator, to balance the intensity through the reference and sensor arms. Figure 11 also shows examples of a successful (uniform attenuation) and unsuccessful (localized attenuation) loading of the POF. Both photographs were taken near the elastic limit of the POF.

The calibrated linear, $(1/L)(\mathrm{d}\varphi/\mathrm{d}\epsilon)$, and nonlinear, $(1/L)(\mathrm{d}^2\varphi/\mathrm{d}\epsilon^2)$, axial strain sensitivities were 1.37×10^7 rad m^{-1} and 3.1×10^6 rad m^{-1} respectively. The linear coefficient was consistent with the measurement of Silva-Lopez *et al* [7]. It was demonstrated that the contribution of the photoelastic nonlinearity is of the same order of magnitude as the finite deformation for the PMMA optical fiber and

therefore cannot be neglected in predicting the sensor response to strain.

Abdi *et al* [29] applied the in-fiber POF Mach–Zehnder interferometer to a tensile specimen and compared the sensor performance to an independent strain measurement from an extensionmeter. For this experiment, the reference arm was a silica optical fiber and the phase response was measured with a 3×3 coupler interrogator [53]. The 3×3 coupler arrangement was modified to permit the extraction of the changing intensity in the sensor arm that would be expected near the elastic strain limit of the POF. The POF was loaded in a single cycle up to 10% elongation and confirmed the extensionmeter measurements. The phase shift–strain response was extremely repeatable between specimens, and no hysteresis was observed at cycles up to 4% elongation. The nonlinearity was greater than that predicted in the formulation of Kiesel *et al* [18, 52], presumably due to the behavior of the adhesive bonding of the POF to the tensile specimen.

5.2. Fiber grating sensors

As for silica based optical fiber sensors, there is a need for localized strain and temperature sensors that can be multiplexed along an optical fiber. For example, Kuang *et al* [54] created a Fabry–Perot interferometer through an air gap between two multi-mode POFs. Although multiple modes interfered in the gap, the response of the Fabry–Perot interferometer was sufficiently coherent to measure changes in the gap length. With the emergence of single-mode POFs, grating structures can now be written in POFs to create intrinsic, localized sensors.

Xiong *et al* [55] first demonstrated the writing of fiber Bragg gratings (FBGs) in polymer optical fibers through photosensitivity. The FBGs were fabricated by UV exposure of PMMA, single-mode optical fibers with dye-doped cores to increase the photosensitivity of the polymer. Liu *et al* [56] later wrote FBGs operating in near IR wavelengths ($\lambda_B \approx$ 1570 nm) with a transmission loss of >28 dB and a bandwidth of <0.5 nm. By applying tensile strain to the FBG, the authors shifted the Bragg wavelength by a total of 52 nm [57], which is an order of magnitude larger than that previously achieved with FBGs in silica optical fibers in pure tension. The large wavelength shift was partially due to the increased strain sensitivity of the polymer optical fiber and partially due to the large yield strain of the POF. Reflection spectra measured from the polymer FBG during loading are plotted in figure 12. No significant changes to the reflected spectra occurred at strain magnitudes below 2.2%. Starting at 2.2% the maximum reflectivity began to decrease and the spectrum broadened. At a tensile strain of approximately 3%, peak-splitting appeared in the reflected spectrum. At a tensile strain of 3.61% the authors considered the reflectivity loss of 4 dB to be too severe to continue loading of the POF.

The authors supposed that the change in reflected spectrum was due to strain non-uniformities appearing along the FBG. The original reflected spectrum was recovered after unloading of the POF. A second interpretation would be that above 2.22% tensile strain, constriction of the POF

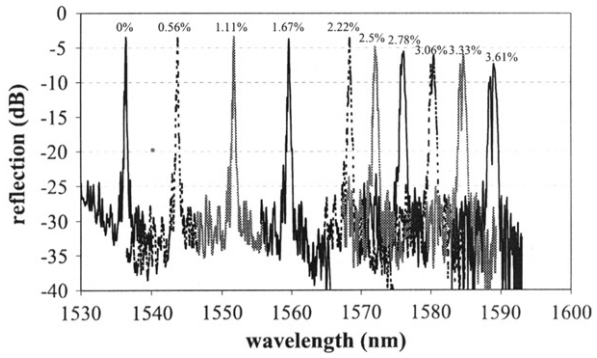

Figure 12. Reflection spectra of polymer FBG due to mechanical tensile loading of the POF. Per cent tensile strain values are indicated for each measurement [57].

cross-section began, as previously observed for multi-mode POFs [32] and discussed in section 3.2. Such constriction would result in mode splitting in the FBG and reflected spectra similar to those seen in figure 12. In agreement with these observations is the fact that no hysteresis was observed after 20 cycles of strain loading up to 2.22%, whereas it was observed for higher strain magnitudes.

The measured Bragg wavelength peak shift was linear with applied strain and an effective photoelastic constant, $p_e = 0.05$, was fit to the measured FBG response [57]. A comparable value for a single-mode silica optical fiber is $0.22 < p_e < 0.24$. As the Bragg wavelength shift, $\Delta\lambda_B$, is related to the strain through

$$\frac{\Delta\lambda_B}{\lambda_B} = (1 - p_e)\epsilon \tag{4}$$

where λ_B is the unloaded Bragg wavelength, the POF demonstrated a 22% increase in sensitivity as compared to a silica optical fiber POF of the same Bragg wavelength.

Applying thermal loading, the authors also tuned the FBG over 18 nm with a temperature change of 50 °C [58]. No hysteresis was observed during cyclic thermal loading. However, erasing of the FBG can occur when the grating is exposed to thermal loads for extended periods of time. The process of thermal erasing is not fully understood for FBGs in POFs. The physical mechanisms for grating fabrication is different in POFs than in silica optical fibers. In POFs the dominant mechanism is through photopolymerization, whereas in silica optical fibers it is through trapping of the ultraviolet excited charge carriers [58]. Similar to the writing process for FBGs in silica fibers, the grating depth increases with exposure time until a threshold is reached at which point damage to the polymer fiber occurs and transmission losses are introduced in the fiber [59]. On the other hand, Liu *et al* [60] observed that when FBGs were written with lower power UV exposures, the FBG peak depth increased, reached a maximum, remained constant, then began to erase during the exposure time. Once the FBG was completely erased the UV exposure was stopped and the FBG re-appeared over a period of 8 h, then was permanent and stable. The authors speculate that the heating of the fiber during the UV exposure temporarily changed the index of refraction, counteracting the change due to photosensitivity.

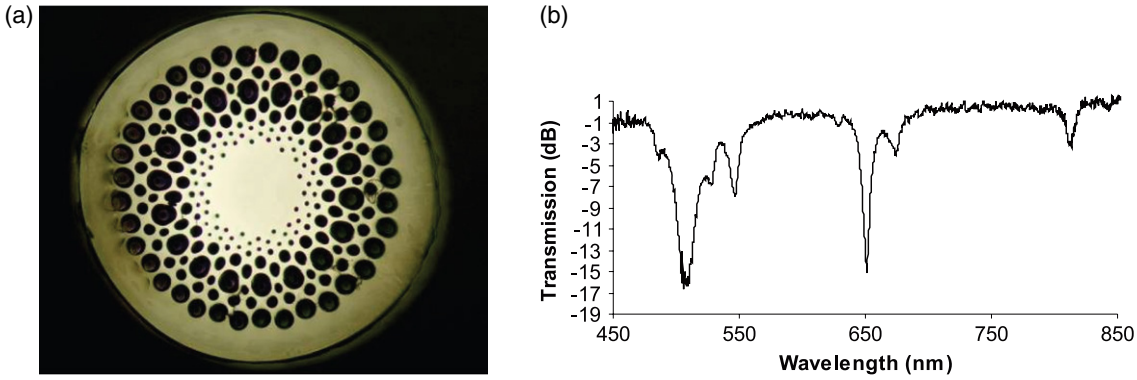

Figure 13. (a) Cross-section of typical microstructured POF [8]. (b) Transmission spectrum of LPG inscribed by heat imprinting of mPOF [69].

Liu *et al* [61] combined FBG sensors in silica and PMMA optical fibers in series to independently measure strain and temperature, through the equation

$$\begin{pmatrix} \Delta\lambda_{\mathrm{p}} \\ \Delta\lambda_{\mathrm{s}} \end{pmatrix} = \begin{pmatrix} K_{\epsilon\mathrm{p}} & K_{T\mathrm{p}} \\ K_{\epsilon\mathrm{s}} & K_{T\mathrm{s}} \end{pmatrix} \begin{pmatrix} \epsilon \\ \Delta T \end{pmatrix} \tag{5}$$

where the $\boldsymbol{K}$ matrix is constructed of the sensitivities of the Bragg wavelength shifts of the FBGs in the polymer ($\Delta\lambda_{\mathrm{p}}$) and silica ($\Delta\lambda_{\mathrm{s}}$) fibers to strain and temperature. These measurements are significantly better than those previously obtained using two FBGS in silica fibers at different wavelengths due to the fact that the sensitivity to strain and temperature are very different for the polymer and silica materials. The measured strain sensitivities were $K_{\epsilon\mathrm{p}} = 1.48\ \mathrm{pm}/\mu\epsilon$ for the PMMA FBG and $K_{\epsilon\mathrm{s}} = 1.15\ \mathrm{pm}/\mu\epsilon$ for the silica FBG. Additionally, the temperature sensitivity of the silica FBG is positive, while the temperature sensitivity of the PMMA FBG is negative. In a similar arrangement, Zhang *et al* [62] combined silica and PMMA FBG sensors to independently measure temperature and humidity. In this work, the differentiation between the two parameters was even stronger, due to the low sensitivity of silica and high sensitivity of PMMA to humidity.

Li *et al* [63] wrote long period gratings in low-mode POFs through photo-etching of the PMMA POF cladding. Although the POF was low-mode at the wavelength of the grating resonance ($\lambda = 1570$ nm), interference between multiple modes was not observed. Such a long period grating could also be applied as a strain/temperature sensor, however Li *et al* [63] did not measure the sensitivity of the grating resonance to these parameters.

Other researchers have used the material flexibilities of POFs to write FBGs with unusual properties. Luo *et al* [64, 65] wrote fiber Bragg gratings and long period gratings in a multi-mode POF (10 modes propagated at the wavelength 632.8 nm) with a azopolymer core. The azopolymer exhibits photoinduced birefringence that can be written using linearly polarized light and then removed using circularly polarized light. In this manner, a Bragg grating was written and erased in the POF repeatedly through eight cycles. Recently, fiber Bragg gratings have also been successfully written into microstructured polymer optical fibers. These sensors will be presented in section 5.3.

5.3. Microstructured POF sensors

Researchers at the University of Sydney first fabricated microstructured polymer optical fibers (mPOFs) to overcome the high intrinsic attenuation properties of common polymers [16]. Microstructured POFs (also known as 'holey fibers') guide light due to a hole pattern in the fiber cross-section. An example mPOF cross-section is shown in figure 13(a). A review of the properties of mPOFs is beyond the scope of this article, however an extensive description can be found in [8]. For sensing applications, the advantages of mPOFs over conventional, solid core optical polymer optical fibers are: (1) as the lightwave propagates through less material in the cross-section, the intrinsic attenuation is potentially lower; (2) due to the difference in guiding properties, a mPOF can be single-mode for a wide range of wavelengths ranging from the visible to near-infrared and (3) this single-mode property is obtained without an extremely small core size, which increases the coupling efficiency to and from the POF.

Dobb *et al* [66] first successfully wrote FBGs in both low-mode and single-mode mPOFs through ultraviolet (UV) inscription. A high intensity exposure of the POF to the UV light was required to compensate for the scattering losses at the hole–air interfaces. The amount of scattering, and therefore the success of the FBG inscription, was highly dependent on the orientation of the microstructure relative to the writing UV beam. The resulting grating had a Bragg wavelength of 1536 nm and a length of 10 mm. When axial strain was applied to the FBG the Bragg wavelength was shifted 41 nm (at a maximum strain just below 3%), at which point the spectral width of the source was reached [8]. The actual upper strain tuning limit of the mPOF FBG is not known. Some hysteresis was observed in the wavelength shift after unloading. Carroll *et al* [67] later measured the temperature sensitivity of similar FBGs. In unannealed mPOFs, the temperature sensitivity was up to $-95\ \mathrm{pm}\ ^{\circ}\mathrm{C}^{-1}$. However, the sensitivity of the unannealed mPOF also showed a high degree of nonlinearity and hysteresis that make it difficult to apply for sensing applications. Therefore, Carroll *et al* [67] repeated the temperature testing on annealed mPOFs, which demonstrated a temperature sensitivity of $-52\ \mathrm{pm}\ ^{\circ}\mathrm{C}^{-1}$, still much higher than comparable silica optical fibers. This temperature sensitivity

was comparable to that measured for FBGs in solid core PMMA POFs (−55 pm °C^{-1}) [62]. The temperature response of the annealed mPOFs was also linear and repeatable without observed hysteresis, ideal for sensing applications.

Recently, long period gratings (LPGs) have also become of interest as localized sensors in mPOFs. LPGs are easier to fabricate than Bragg gratings since the period of the grating is much larger and the periodic structure is imprinted on the outer cladding of the optical fiber. Furthermore, in contrast to LPGs in solid optical fibers, the microstructure of mPOFs can be specifically designed to create specific cladding mode behaviors that are especially sensitive to the parameters of interest [8]. This design can be through the geometry of the hole pattern in the fiber cross-section or through the introduction of fluids into the holes themselves.

van Eijkelenborg *et al* [68] first wrote temporary long period gratings in mPOFs through stress induced changes in the polymer index of refraction by applying a grooved rod to the outer surface of a mPOF. Strong resonance loss peaks were observed (with a maximum loss of 34 dB) in the visible wavelength range. To create a permanent LPG, Hiscocks *et al* [69] heated the grooved rod such that thermally induced residual stresses remained in the POF after the rod was removed. The behavior of these permanent LPGS were tested under various loading, temperature and heating conditions [6, 70]. The shift in LPG resonance demonstrated a linear response up to 0.5% strain with a sensitivity of −10.9 nm/%ϵ. Strong resonance peaks were resolved up to a maximum of 15% strain, consistent with the upper limit in coherent lightwave propagation measured by Kiesel *et al* [52]. Plastic strain was also measured once the strain was removed from the mPOF. The measured sensitivity to relative humidity (RH) was 0.02 nm/%RH.

6. Conclusions and outlook

Recent advances in polymer optical fiber and interrogator technology have led to POF based sensors that are rapidly enabling high deformation, high accuracy optical fiber based strain and temperature sensing. Field applications with multi-mode POFs have also demonstrated their compatibility with structural applications.

Fields where POF sensors will have strong near term impacts are most likely to be the monitoring of large structures or geotechnical foundations where low cost monitoring of large areas can be achieved. While still maintaining the advantages of silica optical fiber sensors, POF based sensors also provide the flexibility to be integrated into complex structural geometries. Such deformation capabilities have been applied to the measurement of crack openings in concrete, the deformation of soil structures and the deformation of textiles. These are all applications where silica based optical fiber sensors present limitations. The introduction of new POF fiber types and materials also has great promise for the near future. While still at a development stage, the potential for polymer fiber Bragg grating sensors or microstructured POF sensors that can deform along with a flexible structure could be incorporated into thin film sensing devices or structural skins for a variety of aerospace, marine and civil engineering applications.

Finally, this article emphasizes the importance of including strain rate and environmental conditions in the calibration of the response of POF sensors. Furthermore, it is important to calibrate the specific POF type to be applied as a sensor because of the differences in material properties, which vary considerably more than those of equivalent silica based optical fiber sensors.

References

[1] Ziemann O, Krauser J, Zamzow P E and Daum W 2008 *POF Handbook* (Berlin: Springer) chapter 8

[2] Measures R M 2001 *Structural Monitoring with Fiber Optic Technology* (San Diego, CA: Academic)

[3] Zubia J and Arrue J 2001 Plastic optical fibers: an introduction to their technological processes and applications *Opt. Fiber Technol.* **7** 101–40

[4] Bartlett R J, Philip-Chandy R, Eldridge P, Merchant D F, Morgan R and Scully P J 2000 Plastic optical fibre sensors and devices *Trans. Inst. Meas. Control* **22** 431–57

[5] Ziemann O, Krauser J, Zamzow P E and Daum W 2008 *POF Handbook* (Berlin: Springer) chapter 2

[6] Large M C J, Moran J and Ye L 2009 The role of viscoelastic properties in strain testing using microstructured polymer optical fibres (mPOF) *Meas. Sci. Technol.* **20** 034014

[7] Silva-López M, Fender A, MacPherson W N, Barton J S, Jones J D C, Zhao D, Dobb H, Webb D J, Zhang L and Bennion I 2005 Strain and temperature sensitivity of a single-mode polymer optical fiber *Opt. Lett.* **30** 3129–31

[8] Large M C J, Poladian L, Barton G W and van Eijkelenborg M A 2007 *Microstructured Polymer Optical Fibers* (Berlin: Springer)

[9] Ghatak A and Thyagarajan K 1998 *Introduction to Fiber Optics* (Cambridge: Cambridge University Press)

[10] Koike Y 1992 High bandwidth and low loss polymer optical fiber *Proc. First Int. Conf. on Plastic Optical Fibres and Applications (Paris)* pp 15–9

[11] Kuzyk M G, Paek U C and Dirk C W 1991 Guest–host polymer fibers for nonlinear optics *Appl. Phys. Lett.* **59** 902–4

[12] Bosc D and Toinen C 1993 Tensile mechanical properties and reduced internal stresses of polymer optical fiber *Polym. Compos.* **14** 410–3

[13] Garvey D W *et al* 1996 Single-mode nonlinear-optical polymer fibers *J. Opt. Soc. Am.* A **13** 2017–23

[14] Kuzyk M G 2007 *Polymer Fiber Optics: Materials, Physics and Applications* (Boca Raton, FL: CRC/Taylor and Francis)

[15] Large M C J, Argyros A, Cox F, van Eijkelenborg M A, Ponrathnam S, Pujari N, Bassett I M, Lwin R and Barton G W 2006 Microstructured polymer optical fibres: new opportunities and challenges *Mol. Cryst. Liq. Cryst.* **446** 219–31

[16] van Eijkelenborg M A *et al* 2001 Microstructured polymer optical fibre *Opt. Express* **9** 319–27

[17] Jiang C, Kuzyk M G, Ding J L, Johns W E and Welker D J 2002 Fabrication and mechanical behavior of dye-doped polymer optical fiber *J. Appl. Phys.* **92** 4–12

[18] Kiesel S, Peters K, Hassan T and Kowalsky M 2007 Behaviour of intrinsic polymer optical fibre sensor for large-strain applications *Meas. Sci. Technol.* **18** 3144–54

[19] Yang D X, Yu J, Tao X and Tam H 2004 Structural and mechanical properties of polymeric optical fiber *Mater. Sci. Eng.* A **364** 256–9

[20] Law S H, van Eijkelenborg M A, Barton G W, Yan C, Lwin R, Gan J and Large M C J 2006 Cleaved end-face quality of microstructured polymer optical fibres *Opt. Commun.* **265** 513–20

[21] Dugas J and Maurel G 1992 Mode-coupling processes in polymethyl methacrylate-core optical fibers *Appl. Opt.* **31** 5069–79

[22] Ziemann O, Krauser J, Zamzow P E and Daum W 2008 *POF Handbook* (Berlin: Springer) chapter 9

[23] Ziemann O, Daum W, Bräuer A, Schlick J and Frank W 2000 Results of a German 6.000 h accelerated aging test of PMMA POF and consequences for the practical use of POF *Proc. POF 2000 (Boston)* pp 133–7

[24] Ziemann O, Krauser J, Zamzow P E and Daum W 2008 *POF Handbook* (Berlin: Springer) chapter 3

[25] Canning J, Buckley E, Groothoff N, Luther-Davies B and Zagari J 2002 UV laser cleaving of air–polymer structured fibre *Opt. Commun.* **202** 139–43

[26] Law S H, Harvey J D, Kruhlak R J, Song M, Wu E, Barton G W, van Eijkelenborg M A and Large M C J 2006 Cleaving of microstructured polymer optical fibres *Opt. Commun.* **258** 193–202

[27] Abdi O, Wong K C, Hassan T, Peters K J and Kowalsky M J 2009 Cleaving of single mode polymer optical fiber for strain sensor applications *Opt. Commun.* **282** 856–61

[28] Kiesel S, Peters K, Hassan T and Kowalsky M 2008 Large deformation in-fiber polymer optical fiber sensor *IEEE Photon. Technol. Lett.* **20** 416–8

[29] Abdi O, Kowalsky M, Peters K and Hassan T 2010 Tensile testing of a single mode, polymer optical fiber large deformation strain sensor *Meas. Sci. Technol.* submitted

[30] Lwin R and Argyros A 2009 Connecting microstructured polymer optical fibres to the world *Proc. 18th Int. Conf. on Plastic Optical Fibers and Applications (Sydney)*

[31] Kiesel S, Van Vickle P, Peters K, Abdi O, Hassan T and Kowalsky M 2006 *Proc. SPIE Sensors and Smart Structures Technologies for Civil, Mechanical, and Aerospace Systems (San Diego)*; *Proc. SPIE* **6174** 617435

[32] Liehr S, Lenke P, Wendt M, Drebber K, Seeger M, Thiele E, Metschies H, Gebreselassie B and Münich J C 2009 Polymer optical fiber sensors for distributed strain measurement and application in structural health monitoring *IEEE Sensors J.* **9** 1330–8

[33] Schukar M, Grzemba B, Krebber K and Luber M 2009 Integration technology of POF sensors into composites for structural health monitoring *Proc. 18th Int. Conf. on Plastic Optical Fibers and Applications (Sydney)*

[34] Takeda N 2002 Characterization of microscopic damage in composite laminates and real-time monitoring by embedded optical fiber sensors *Int. J. Fatigue* **24** 281–9

[35] Kuang K S C, Cantwell W J and Scully P J 2002 An evaluation of a novel plastic optical fibre sensor for axial strain and bend measurements *Meas. Sci. Technol.* **13** 1523–34

[36] Kuang K S C and Cantwell W J 2003 The use of plastic optical fibres and shape memory alloys for damage assessment and damping control in composite materials *Meas. Sci. Technol.* **14** 1305–13

[37] Kuang K S C, Akmaluddin, Cantwell W J and Thomas C 2003 Crack detection and vertical deflection monitoring in concrete beams using plastic optical fibre sensors *Meas. Sci. Technol.* **14** 205–16

[38] Wong Y M, Scully P J, Bartlett R J, Kuang K S C and Cantwell W J 2003 Plastic optical fibre sensors for environmental monitoring: biofouling and strain applications *Strain* **39** 115–9

[39] Chen Y C, Xie W F, Ke Y L and Chen L W 2008 Power loss characteristics of a sensing element based on a grooved polymer optical fiber under elongation *Meas. Sci. Technol.* **19** 105203

[40] Babchenko A, Weinberger Z, Itzkovich N and Maryles J 2006 Plastic optical fibre with structural imperfections as a displacement sensor *Meas. Sci. Technol.* **17** 1157–61

[41] Remouche M, Mokdad R, Chakari A and Meyrueis P 2007 Intrinsic integrated optical temperature sensor based on waveguide bend loss *Opt. Laser Technol.* **39** 1454–60

[42] Husdi I R, Nakamura K and Ueha S 2004 Sensing characteristics of plastic optical fibres measured by optical time-domain reflectometry *Meas. Sci. Technol.* **15** 1553–9

[43] Nakamure K, Husdi I R and Ueha S 2004 Memory effect of POF distributed strain sensor *Proc. SPIE 5502 Second European Workshop on Optical Fiber Sensors (Santander)* pp 144–7

[44] Krebber K, Lenke P, Liehr S, Witt J and Schukar M 2008 Smart technical textiles with integrated POF sensors *Proc. SPIE Smart Sensor Phenomena, Technology, Networks and Systems (San Diego, CA)*; *Proc. SPIE* **6933** 69330V

[45] Gillet A, Kinet D, Witt J, Schukar M, Krebber K, Pirotte F and Depré A 2008 Optical fiber sensors embedded into medical textiles for healthcare monitoring *IEEE Sensors J.* **8** 1215–22

[46] Liehr S, Nöther N and Krebber K 2010 Incoherent optical frequency domain reflectometry and distributed strain detection in polymer optical fibers *Meas. Sci. Technol.* **21** 017001

[47] Liehr S and Krebber K 2010 A novel quasi-distributed fibre optic displacement sensor for dynamic measurement *Meas. Sci. Technol.* **21** 075205

[48] Kreger S, Sang A K, Gifford D K and Froggatt M E 2009 Distributed strain and temperature sensing in plastic optical fiber using Rayleigh scatter *Fiber Optic Sensors and Applications VI (Orlando, FL)*; *Proc. SPIE* **7316** 73160A

[49] Gomez J, Zubia J, Aranguren G, Arrue J, Poisel H and Saez I 2009 Comparing polymer optical fiber, fiber Bragg grating, and traditional strain gauge for aircraft structural health monitoring *Appl. Opt.* **48** 1436–43

[50] Durana G, Kirchhof M, Luber M, Sáez de Ocáriz I, Poisel H, Zubia J and Vázquez C 2009 Use of a novel fiber optical strain sensor for monitoring the vertical deflection of an aircraft flap *IEEE Sensors J.* **9** 1219–25

[51] Jiang G, van Vickle P, Peters K and Knight V 2007 Oscillator interrogated time-of-flight fiber interferometer for global strain measurements *Sensors Actuators* A **135** 443–50

[52] Kiesel S, Peters K, Hassan T and Kowalsky M 2009 Calibration of a single-mode polymer optical fiber large-strain sensor *Meas. Sci. Technol.* **20** 034016

[53] Koo K P, Tveten A B and Dandridge A 1982 Passive stabilization scheme for fiber interferometers using (3 × 3) fiber directional couplers *Appl. Phys. Lett.* **41** 616–8

[54] Kuang K S C, Quek S T and Maalej M 2004 Assessment of an extrinsic polymer-based optical fibre sensor for structural health monitoring *Meas. Sci. Technol.* **15** 2133–41

[55] Peng G D, Xiong Z and Chu P L 1999 Photosensitivity and gratings in dye-doped polymer optical fibers *Opt. Fiber Technol.* **5** 242–51

[56] Liu H Y, Peng G D and Chu P L 2002 Polymer fiber Bragg gratings with 28 dB transmission rejection *IEEE Photon. Technol. Lett.* **14** 935–7

[57] Liu H Y, Liu H B and Peng G D 2005 Tensile strain characterization of polymer optical fibre Bragg gratings *Opt. Commun.* **251** 37–43

[58] Liu H Y, Peng G D and Chu P L 2001 Thermal tuning of polymer optical fiber Bragg gratings *IEEE Photon. Technol. Lett.* **13** 824–6

[59] Liu H Y, Liu H B, Peng G D and Chu P L 2003 Observation of type I and type II gratings behavior in polymer optical fiber *Opt. Commun.* **220** 337–43

[60] Liu H B, Liu H Y, Peng G D and Chu P L 2004 Novel growth behaviors of fiber Bragg gratings in polymer optical fiber under UV irradiation with low power *IEEE Photon. Technol. Lett.* **16** 159–61

[61] Liu H B, Liu H Y, Peng G D and Chu P L 2003 Strain and temperature sensor using a combination of polymer and silica fibre Bragg gratings *Opt. Commun.* **219** 139–42
[62] Zhang C, Zhang W, Webb D J and Peng G D 2010 Optical fibre temperature and humidity sensor *Electron. Lett.* **46** 643–4
[63] Li Z, Tam H Y, Xu L and Zhang Q 2005 Fabrication of long-period gratings in poly(methyl methacrylate-co-metthyl vinyl ketone-co-benzyl methacrylate)-core polymer optical fiber by use of a mercury lamp *Opt. Lett.* **30** 1117–9
[64] Luo Y, Zhou J, Yan Q, Su W, Li Z, Zhang W, Huang J and Wang K 2007 Optical manipulable polymer optical fiber Bragg gratings with azopolymer as core material *Appl. Phys. Lett.* **91** 071110
[65] Luo Y, Li Z, Zheng R, Chen R, Yan Q, Zhang Q, Peng G, Zou G, Ming H and Zhu B 2009 Birefringent azopolymer long period fiber gratings induced by 532 nm polarized laser *Opt. Commun.* **282** 2348–53
[66] Dobb H, Webb D J, Kalli K, Argyros A, Large M C J and van Eijkelenborg M A 2005 Continuous wave ultraviolet light-induced fiber Bragg gratings in few- and single-mode microstructured polymer optical fibers *Opt. Lett.* **30** 3296–8
[67] Carroll K E, Zhang C, Webb D J, Kalli K, Argyros A and Large M C J 2007 Thermal response of Bragg gratings in PMMA microstructured optical fibers *Opt. Express* **15** 8844–50
[68] van Eijkelenborg M A, Padden W and Besley J A 2004 Mechanically induced long-period gratings in microstructured polymer fibre *Opt. Commun.* **236** 75–8
[69] Hiscocks M P, van Eijkelenborg M A, Argyros A and Large M C J 2006 Stable imprinting of long-period gratings in microstructured polymer optical fibre *Opt. Express* **14** 4644–7
[70] Steffen M, Schukar M, Witt J, Krebber K, Large M and Argyros A 2009 Investigation of MPOF–LPGs for sensing applications *Proc. 18th Int. Conf. on Plastic Optical Fibers and Applications (Sydney)*